Faraday Discuss. Chem. Soc., 1991, **91**, 289-304

Quantum-dynamical Characterization of Reactive Transition States

David C. Chatfield, Ronald S. Friedman and Donald G. Truhlar
Department of Chemistry and Supercomputer Institute, University of Minnesota, Minneapolis, MN 55455-0431, USA

David W. Schwenke
NASA Ames Research Center, Moffet Field, CA 94035, USA

It is shown that the accurate quantum-mechanical probability of the reaction of H with H_2, with either zero or one unit of total angular momentum, increases with energy by increments of resolvable 'quanta' of reactive flux. These are analysed in terms of quantized transition states. Bend and stretch quantum numbers are assigned for total angular momentum J equal to zero and for both parities for $J = 1$ based on an analysis of the density of reactive states. A more detailed description of the reactive scattering process has been obtained by examining the state-selected densities of reactive states, and the initial $H + H_2$ channels that contribute to the reactive flux passing through specific transition states have been determined.

1. Introduction

In recent work,[1] we showed that the quantum-mechanical probability of reaction of H with H_2 is globally controlled by quantized transition states up to very high energies, including the entire range of energies relevant to thermal rate constants for the $H + H_2$ reaction. This finding provides strong support for the assumptions of approximate methods, such as variational transition-state theory,[2] which employ conventional or generalized transition states in the calculation of rate constants. Our analysis was based upon step-like features[1,3] in the cumulative reaction probability (CRP) as a function of energy, each of which we demonstrated was due to the energetic threshold for a quantized dynamical bottleneck, or transition state, gating the flow of reactive flux from reactants to products. We were able to assign quantum numbers to the modes of motion orthogonal to the reaction coordinate.

The quantum-mechanical CRP, denoted for a particular value of total angular momentum J, parity P, and total energy E by $N^{JP}_{\alpha\alpha'}(E)$, is defined as the sum over all state-to-state ($n \rightarrow n'$) reactive transition probabilities $P^{JP}_{\alpha n\alpha' n'}(E)$ from a given initial chemical arrangement α to a final chemical arrangement α':

$$N^{JP}_{\alpha\alpha'}(E) = \sum_{n} \sum_{n'} P^{JP}_{\alpha n\alpha' n'}(E) \tag{1}$$

where n denotes the collection of all initial quantum numbers, and n' denotes the set of final ones. For example, for an atom–diatom reaction, $A + BC \rightarrow AB + C$, $n(n')$ denotes the collection of the initial (final) vibrational quantum number $v(v')$, rotational quantum number $j(j')$, and orbital angular momentum quantum number $l(l')$. The CRP holds all the dynamical information needed to calculate an ordinary temperature-dependent rate coefficient $k(T)$. In particular, for a canonical ensemble at

temperature T[4-6]

$$k(T) = \frac{\sum_J \sum_P (2J+1) \int_0^\infty \mathrm{d}E \exp(-E/k_B) N_{\alpha\alpha'}^{JP}(E)}{\Phi^R(T)} \tag{2}$$

where k_B is Boltzmann's constant, and $\Phi^R(T)$ is the reactants' partition function per unit volume at temperature T.

In both our previous paper[1] (referred to as paper I) and this one, we centre our attention on the density of reactive states, defined as

$$\rho_{\alpha\alpha'}^{JP}(E) = \mathrm{d}N_{\alpha\alpha'}^{JP}/\mathrm{d}E \tag{3}$$

As we showed in paper I, the quantity $\rho_{\alpha\alpha'}^{JP}$ as a function of E may be interpreted as a generalized-transition-state spectrum.

In paper I, we fit the density curve to a sum of lineshapes appropriate to adiabatic transition-state theory[5,6] with tunnelling through parabolic potential-energy barriers at each variational transition state, as follows:

$$\rho_{\alpha\alpha'}^{JP}(E) = \sum_\tau N_\tau \frac{\exp[(V_\tau - E)/W_\tau]}{W_\tau\{1+\exp[(V_\tau - E)/W_\tau]\}^2} \tag{4}$$

where τ refers to a particular quantized transition state, V_τ is the barrier maximum, W_τ is a width parameter and N_τ is a measure of the amount of reactive flux passing through transition state τ. Parabolas are used only because they are the simplest model available. When tunnelling is neglected or unimportant, adiabatic transition-state theory reduces to variational transition-state theory (VTST) if all $N_\tau = 1$.[6]

We define $N_{\alpha\alpha'}^{J}$ and $\rho_{\alpha\alpha'}^{J}$ as the sums over both parity contributions. For $J=0$, $N_{\alpha\alpha'}^{J} = N_{\alpha\alpha'}^{JP}$ and $\rho_{\alpha\alpha'}^{J} = \rho_{\alpha\alpha'}^{JP}$ since there is only one parity for $J=0$.

All of the features in the quantal density curve for $J=0$ were fitted quite well with ten terms included in the sum.[1] The quantal density curve is shown as the solid line in Fig. 1(*a*). We assigned symmetric stretch (v_1), bend (v_2), and vibrational angular momentum (K) quantum numbers to the thresholds, or quantized transition states, by a combination of methods. The threshold energies obtained by fitting the accurate quantal CRPs agreed quite well for small values of v_2 with semiclassical predictions[1] computed by variational transition-state theory.[2] This indicates that the quantum-mechanical flux, though highly non-adiabatic, is 'focussed' in the interaction region through a sequence of discrete transition states whose energies correlate well with locally adiabatic structures. Furthermore, most of the N_τ values were close to unity, confirming the fundamental assumption of VTST. The thresholds also agree quite well with the energies of time delayed features found in an earlier analysis.[7] A threshold is denoted by its quantum numbers as $[v_1 v_2^K]$. Spectroscopic constants were obtained by fitting the $[00^0]$, $[02^0]$, $[04^0]$, $[10^0]$, $[12^0]$ and $[20^0]$ states for $J=0$ and the $[00^0]$ state for $J=4$ by[8]

$$\begin{aligned} E^{(1)}(v_1, v_2)/hc = {} & E_0/hc + \omega_1(v_1+0.5) + x_{11}(v_1+0.5)^2 + \omega_2(v_2+1) \\ & + x_{22}(v_2+1)^2 + x_{12}(v_1+0.5)(v_2+1) + BJ(J+1) \end{aligned} \tag{5}$$

where E_0 is a constant and ω_1, ω_2, x_{11}, x_{12}, x_{22} and B are the usual spectroscopic fitting parameters. Additional levels predicted by these constants were in good agreement with the other observed thresholds. Vibrationally specific densities of reactive states, defined as

$$\rho_{\alpha v\alpha' v'}^{JP}(E) = \mathrm{d}\left(\sum_{jlj'l'} P_{\alpha vjl\alpha' v'j'l'}^{JP}\right) \Big/ \mathrm{d}E \tag{6}$$

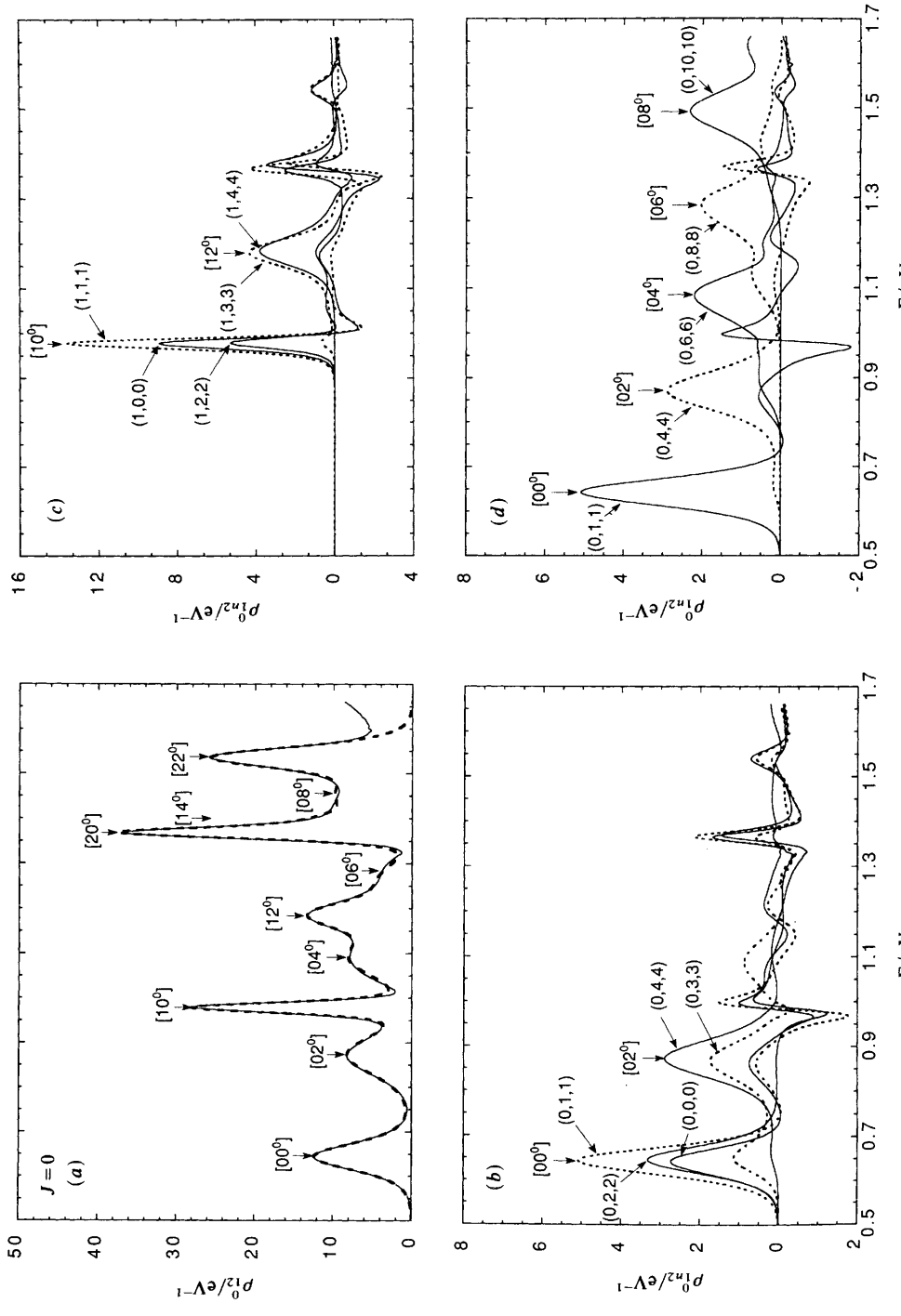

Fig. 1 (*a*) Density of reactive states for $J = 0$. The solid curve is a spline fit to the accurate quantal results and the dashed curve is the fit of eqn. (4). The positions of the fitted thresholds $[v_1 v_2^K]$ are indicated by vertical arrows. (*b*)–(*d*) State-selected densities of reactive states for $J = 0$. Channels are labelled (v, j, l). In (*d*), the most prominent contributor to each $[0v_2^K]$ feature is shown

were used to confirm assignments of quantum numbers to the thresholds by taking advantage of the propensity for the initial vibrational quantum number to correlate with the transverse stretch quantum number of the quantized transition state.

In paper I, we assigned quantum numbers to all of the quantized transition states for $J=0$ up to 1.6 eV and all of the transition states for $J=4$ up to 1.28 eV. In this paper, we identify and assign quantum numbers for all of the quantized transition states for $J=1$ up to 1.6 eV, and we use state-selected densities of reactive states to associate the flux through specific transition states with individual reaction probabilities out of specific reactant states and into specific product states for both $J=0$ and 1. The state-selected densities of reactive states, defined as

$$\rho^{JP}_{\alpha n\alpha' n'}(E) = \mathrm{d}\left(\sum_{n'} P^{JP}_{\alpha n\alpha' n'}\right) \Big/ \mathrm{d}E \tag{7}$$

are used to learn which initial quantum states of the system react most strongly *via* a particular quantized transition state at its energetic threshold. This provides a much more detailed conceptual understanding of the reaction than was previously possible.

2. Calculations

Converged quantum dynamics calculations were carried out using a double many-body expansion (DMBE)[9] of the potential-energy surface. The quantum dynamics calculations were performed with the generalized Newton variational principle and an L^2 expansion of the reactive amplitude density, as described previously.[10] Basis sets and numerical parameters were taken from previous work[11] and were checked for convergence at both low and high energies. We carried out well converged calculations for $J=0$ at 258 energies in the range 0.27–1.66 eV and for $J=1$ at 148 energies in the range 0.30–1.66 eV.

Fig. 1 and 2 show ρ^J_{12} and several ρ^J_{1n2} for $J=0$. Fig. 3 shows N^J_{12}, ρ^J_{12}, and ρ^{JP}_{12} for $J=1$, and Fig. 4 shows ρ^{JP}_{1n2} for several n for $J=1$. All accurate density curves were obtained obtained by analytic differentiation of cubic-spline fits. Several of these figures [1(*a*), 2(*a*)-(*d*), 3(*b*)-(*d*)] also show fits of the form (4) which will be discussed in section 3.

3. Interpretation

The state-to-state reaction probabilities[1,11,12] allow us to examine the degree of vibrational, rotational and orbital adiabaticity in the full chemical reaction. The reaction probabilities demonstrate a propensity for vibrational adiabaticity ($v=v'$); however, many probabilities with $v\neq v'$ are also significant ($>10^{-3}$). Non-adiabaticity is even stronger in the rotational and orbital quantum numbers. However, we have shown in paper I that quantized transition-state energies correlate well with thresholds in vibrationally adiabatic potential-energy curves. Thus we conclude that the dynamics for the full collision of H and H_2 is only *locally* adiabatic in the vicinity of the transition-state thresholds. Local adiabaticity at the transition-state thresholds is consistent with the reaction-coordinate motion being classically stopped there.

Here we examine a more detailed quantity, the propensity for adiabaticity between an initial channel and an individual quantized transition state in half collisions. In adiabatic correlations for half collisions,[13,14] j and l excitations correlate with v_2 excitations, and v correlates with v_1. By studying state-selected densities of reactive states, rather than the cumulative reaction probabilities, we determine which transition states are accessed near their threshold energies by the reactive flux out of a given initial state. (By symmetry, for the present reaction, these results apply equally well to final states.)

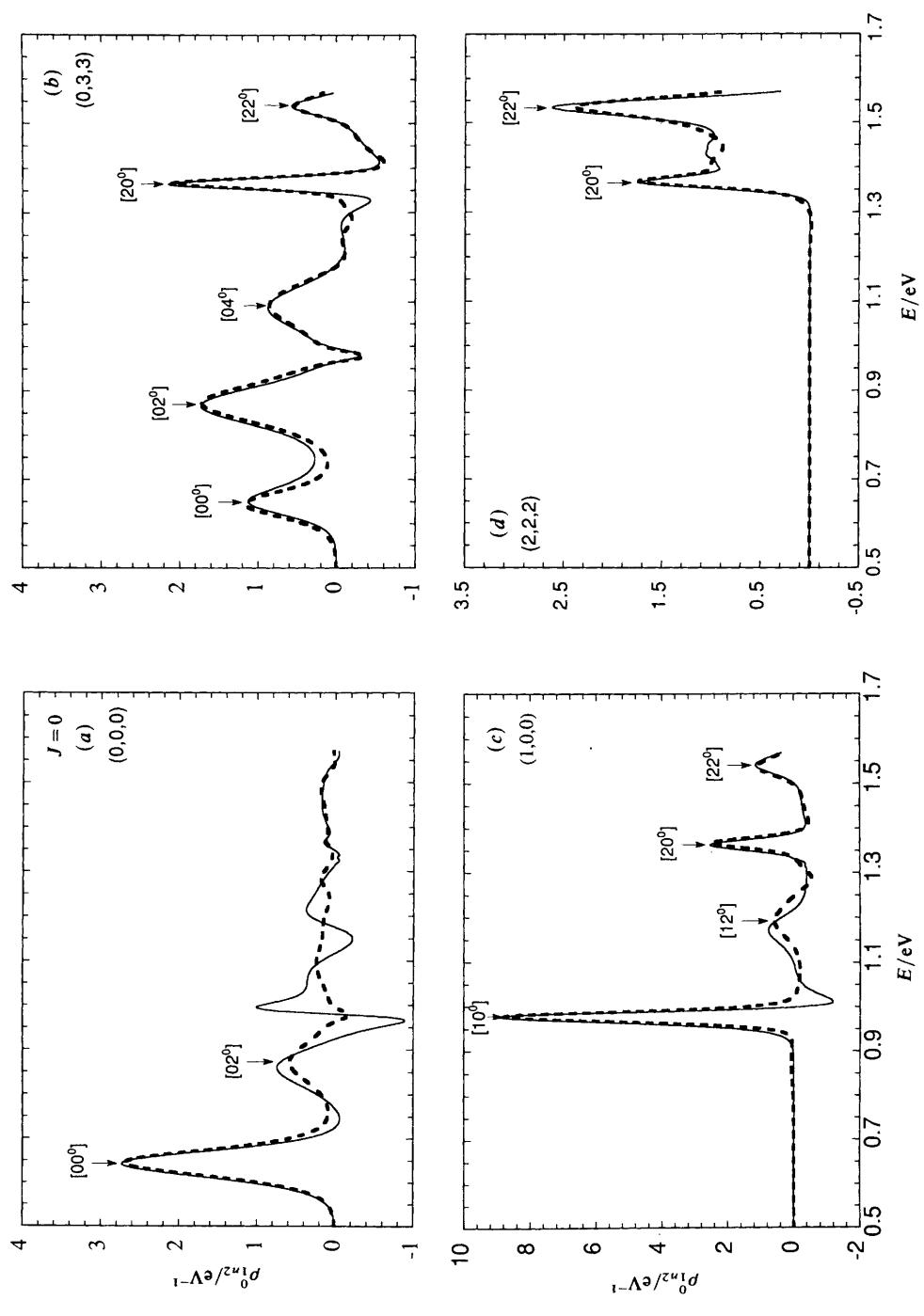

Fig. 2 State-selected densities of reactive states for $J = 0$. Solid curves are spline fits to the accurate quantal results and dashed curves are the fits. Features due to the dominant thresholds $[v_1 v_2^K]$ are indicated. (*a*) Channel (0, 0, 0); (*b*) channel (0, 3, 3); (*c*) channel (1, 0, 0); (*d*) channel (2, 2, 2)

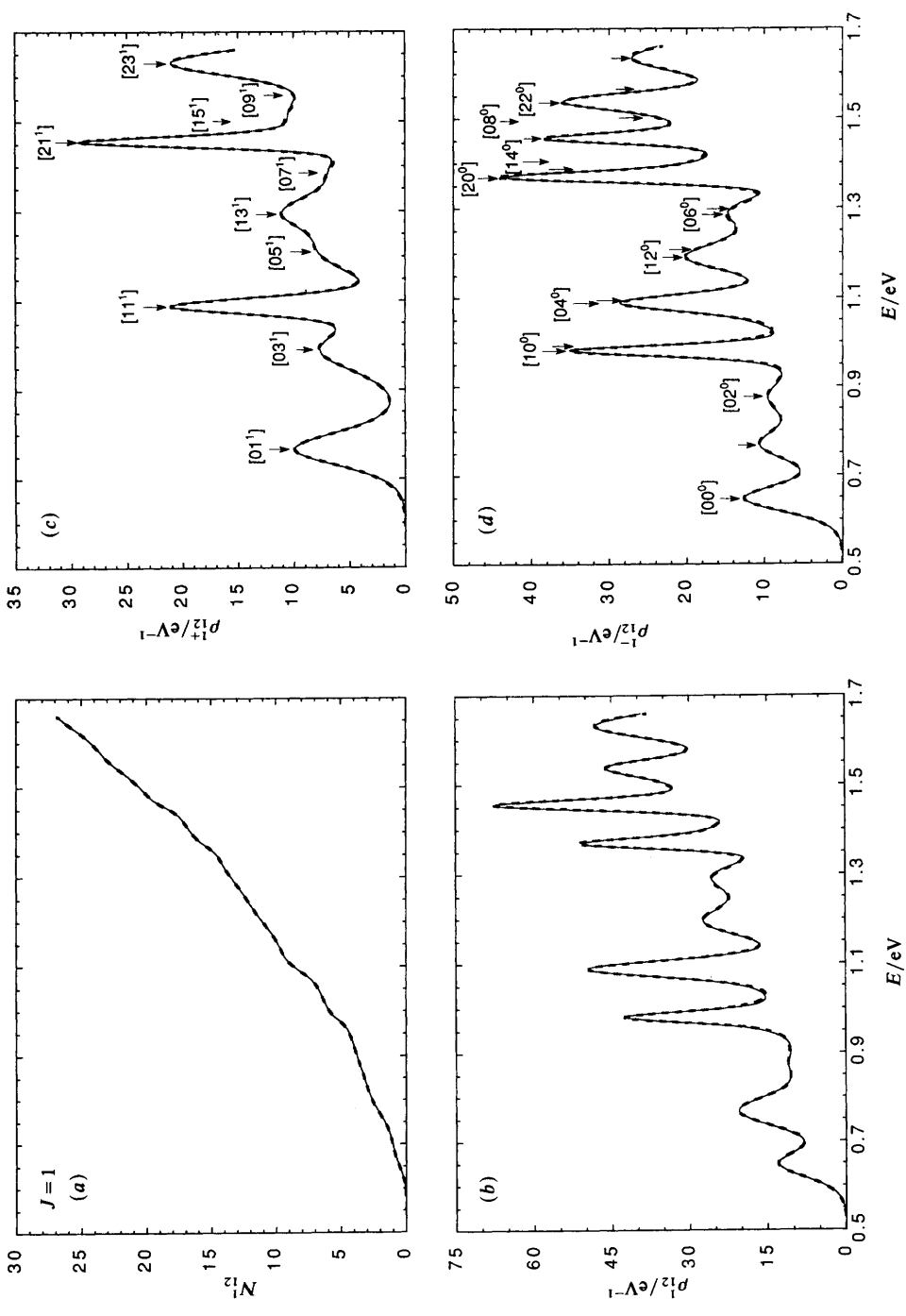

Fig. 3 (*a*) Cumulative reaction probability for $J = 1$. The solid curve is a spline fit to the accurate quantal results and the dashed curve is obtained by integrating the synthetic density curve shown in Fig. 3(*b*). (*b*)-(*d*) Density of reactive states for $J = 1$ in (*b*), $JP = 1+$ in (*c*) and $JP = 1-$ in (*d*). Solid curves are spline fits to the accurate quantal results and dashed curves are the fits. The unlabelled arrows in (*d*) indicate the positions of the fitted thresholds $[v_1 v_2^K]$ which also appear in (*c*)

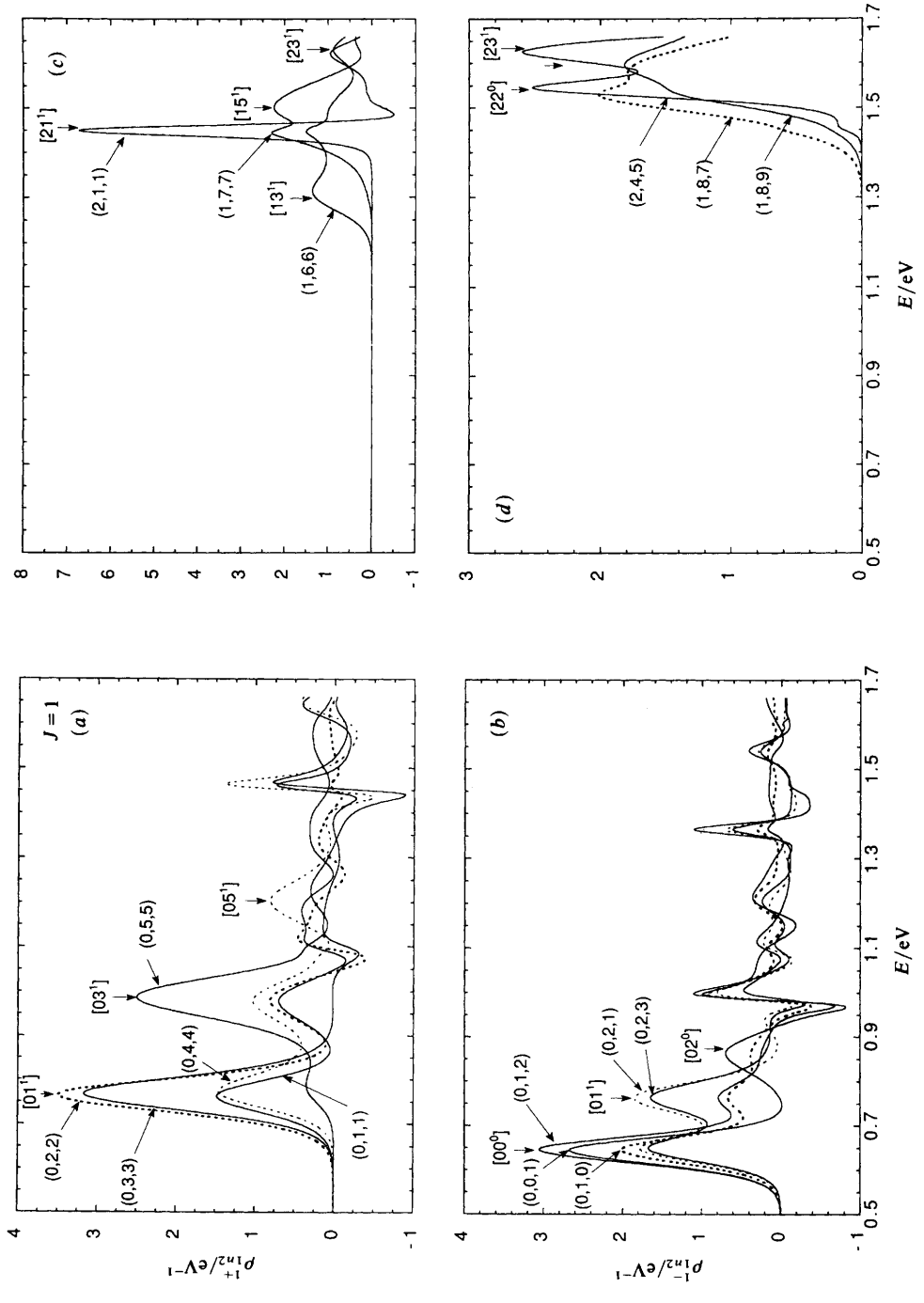

Fig. 4 State-selected densities of reactive states. (*a*), (*c*) $JP = 1+$; (*b*), (*d*) $JP = 1-$. Channels (v, j, l) and thresholds $[v_1 v_2^K]$ are indicated. In (*d*), the unlabelled arrow indicates the position of the maximum in the (1, 8, 9) spectrum

When (v, j, l) channels couple primarily to thresholds $[v_1 v_2^K]$ with $v = v_1$, we denote this as half-collision stretch adiabaticity.

$J = 0$

State-selected reactivity spectra for the five initial channels, labelled (v, j, l), with lowest internal vibrational-rotational-orbital energy are shown in Fig. 1(*b*). These asymptotic channels couple primarily to one or both of the first two transition states, $[00^0]$ and $[02^0]$, displaying a preference for half-collision stretch adiabaticity. Individual initial channels appear to respond to slightly different effective potential-energy barriers for a given quantized transition state, as evidenced by the different energies of the peak maxima. The (0, 0, 0), (0, 1, 1), (0, 2, 2) and (0, 3, 3) spectra all have peak maxima within ±0.007 eV of the fitted threshold energy, 0.645 eV, for the $[00^0]$ state. These four channels peak at successively higher energies, 0.642, 0.644, 0.646 and 0.652 eV. Likewise, the (0, 0, 0), (0, 1, 1), (0, 3, 3) and (0, 4, 4) spectra exhibit local maxima at successively higher energies within a narrow range (±0.012 eV) of the $[02^0]$ threshold energy, 0.872 eV. For both the $[00^0]$ and $[02^0]$ quantized transition states, the threshold energies determined in the fit to the total reactive density agree most closely with the energies of the peak maxima in the state-selected density spectra of the initial channels which contribute most strongly to each threshold, in particular, the (0, 1, 1) and (0, 4, 4) initial channels, respectively.

Fig. 1(*b*) also shows that the channels (0, 0, 0), (0, 1, 1) and (0, 2, 2) most strongly couple to the $[00^0]$ threshold, while the channels (0, 3, 3) and (0, 4, 4) couple predominantly to the $[02^0]$ threshold. It is interesting to note that the (0, 4, 4) channel shows very little coupling to the $[00^0]$ threshold, in spite of the fact that this channel possesses a significant amount of translational energy (0.23 eV, as compared to 0.38, 0.36, 0.33, and 0.29 eV, respectively, for the (0, 0, 0), (0, 1, 1), (0, 2, 2), and (0, 3, 3) channels). Thus it appears that (0, 4, 4)-$[00^0]$ coupling is inhibited by the potential surface rather than by kinematics.

State-selected density spectra for $v = 1$ are shown in Fig. 1*c*; the trends are similar. The (1, 0, 0), (1, 1, 1) and (1, 2, 2) asymptotic channels couple primarily to the $[10^0]$ threshold, while the (1, 3, 3) and (1, 4, 4) channels couple predominantly to the $[12^0]$ threshold. Similar trends are observed in the $v = 2$ state-selected spectra. In general, asymptotic channels couple primarily to one or two consecutive thresholds in the $v_1 = v$ stretch manifold, revealing a high propensity for half-collision stretch adiabaticity.

The regular spacings between the bend levels (v_2) within a given stretch (v_1) manifold are strikingly displayed by plotting together the spectra for those asymptotic channels which contribute most strongly to each threshold within that stretch manifold. Such a plot is shown for $v_1 = 0$ in Fig. 1(*d*). These state-selected spectra bring out this structure even more strikingly than the total reactive density.

The threshold energies for the $[06^0]$ and $[08^0]$ transition states can be more accurately determined from the state-selected spectra than from the total reactive density, where they appear as weak, broad structures overlapping other threshold features. For this reason we repeated the fit[1] to the $J = 0$ density of reactive states keeping the energies V_τ of the $[06^0]$ and $[08^0]$ thresholds fixed at the energies of the maxima in the state-selected spectra for (0, 8, 8) (1.286 eV) and (0, 10, 10) (1.494 eV), respectively [see Fig. 1(*d*)]. Initially, four of the N_τ values, excluding the final one, turned out to be larger than 1, so in a second fit, these four N_τ values were constrained to 1.0, and the fit was repeated still keeping the $[06^0]$ and $[08^0]$ threshold energies fixed. (The final N_τ value should not be interpreted quantitatively because it generally includes significant contributions from neglected higher-energy threshold features.) Finally, the ten pairs of V_τ and W_τ were constrained to the values in the second fit, and all N_τ values were determined by linear least squares. The synthetic density plot from this final fit is shown as a dashed

Table 1 Quantized transition states

	$E^{(1)}(v_1, v_2)$/eV		V_τ/eV		N_τ		$W_\tau/10^{-2}$ eV	
threshold	$J=0$	$J=1$	$J=0$	$J=1$	$J=0$, $JP=1+$[a]	$JP=1-$	$J=0$	$J=1$
$[00^0]$	0.645	0.647	0.645	0.647	1.00	1.00	2.01	2.04
$[01^1]$		0.762		0.767	1.00	0.97		2.53
$[02^0]$	0.872	0.875	0.872	0.875	0.97	1.01	2.95	3.06
$[03^1]$		0.986		0.990	1.01	0.96		3.29
$[04^0]$	1.094	1.096	1.094	1.088	0.98	1.00	3.30	2.16
$[05^1]$		1.205		1.205	0.81	1.00		3.07
$[06^0]$	1.309	1.311	1.286	1.290	0.18	0.79	1.48	2.30
$[07^1]$		1.416		1.388	0.55	0.09		2.74
$[08^0]$	1.517	1.520	1.494	1.498	1.01	1.21	3.02	2.89
$[09^1]$		1.622		1.560	0.27	0.27		2.15
$[0\,10^0]$	1.720	1.722		—[b]		—[b]		—[b]
$[10^0]$	0.978	0.981	0.978	0.981	0.79	0.84	0.75	0.79
$[11^1]$		1.088		1.089	0.98	0.73		1.28
$[12^0]$	1.192	1.194	1.192	1.187	1.02	1.00	2.17	2.19
$[13^1]$		1.299		1.298	1.00	0.39		2.71
$[14^0]$	1.399	1.401	1.405	1.401	0.80	1.21	2.14	2.18
$[15^1]$		1.502		1.502	1.00	0.81		2.75
$[16^0]$	1.599	1.602	—[c]	—[b]	—[c]	—[b]	—[c]	—[b]
$[17^1]$		1.700		—[b]	—[b]	—[b]		—[b]
$[20^0]$	1.368	1.371	1.368	1.370	1.01	1.03	0.78	0.80
$[21^1]$		1.471		1.456	0.74	0.77		0.82
$[22^0]$	1.567	1.570	1.538	1.540	1.15	1.01	1.40	1.28
$[23^1]$		1.667		1.633[d] 1.639[e]	1.91[d]	2.88[e]		2.34[d] 2.73[e]

[a] The $K=0$ values are from the $J=0$ fit and the $K=1$ values from the $JP=1+$ fit. [b] The contribution of this state is believed to be included in the unresolved feature nominally assigned as $[23^1]$. [c] The contribution of this state is believed to be included in the feature nominally assigned as $[22^0]$ in the $J=0$ fit. [d] Values from the $JP=1+$ fit. [e] Values from the $JP=1-$ fit.

line in Fig. 1(*a*), and the threshold parameters V_τ, W_τ, and N_τ are presented in Table 1. Spectroscopic constants for these quantized transition states were obtained by fitting eqn. (5) to the $[00^0]$, $[02^0]$, $[04^0]$, $[10^0]$, $[12^0]$ and $[20^0]$ threshold energies for $J=0$ as obtained from the fit just discussed and the $[00^0]$ energy for $J=4$ from paper I. They were found to be $\omega_1 = 2295\ \text{cm}^{-1}$, $\omega_2 = 972\ \text{cm}^{-1}$, $x_{11} = 227\ \text{cm}^{-1}$, $x_{22} = -6\ \text{cm}^{-1}$, $x_{12} = -58\ \text{cm}^{-1}$ and $B = 10.6\ \text{cm}^{-1}$. The fitted $[06^0]$ and $[08^0]$ threshold energies and the spectroscopically predicted values reported in table 1 show better agreement than was obtained in paper I. This increases our confidence in the threshold energies determined by using the state-selected density spectra.

The state-selected spectra allow further analysis of stretch non-adiabaticity in half collisions. For example, the (0, 0, 0), (0, 1, 1), (0, 2, 2) and (0, 3, 3) spectra all exhibit structure near the $[10^0]$ threshold, and many of the $(0, j, l)$ and $(1, j, l)$ channels appear to couple to the $[20^0]$ threshold. The amount of stretch non-adiabaticity tends to be larger for higher-energy thresholds. A striking example is the (1, 6, 6) spectra, which has a double peak above 1.3 eV, similar to the structure in the (1, 7, 7) curve in Fig. 4(*c*). The first peak corresponds to the $[20^0]$ threshold and the second peak to the $[14^0]$ threshold.

It is interesting to note that several of the $v=0$ state-selected spectra in Fig. 1(*b*) exhibit minima (*i.e.* negative values for ρ^0_{12}) as well as maxima at energies near the $[10^0]$ threshold energy, indicating 'intensity robbing' or possibly the consequences of trapped

states[15] lying very close in energy to thresholds. Further work in this area could shed light on the distinction between trapped states and thresholds.

By inspecting the state-selected density spectra, we have examined the degree of stretch adiabaticity and non-adiabaticity in the half collision of H and H_2. In order to ascertain more quantitatively which initial channels couple to which quantized transition states, we fit each state-selected density spectrum with a sum of lineshapes for tunnelling through parabolic potential-energy barriers, as we did for the total density. Here, however, $N_{\tau n}$ replaces the parameter N_τ of eqn. (4); $N_{\tau n}$ represents a measure of the reactive flux originating from a specific initial (v, j, l) channel and passing through transition state τ at its threshold energy. We fix the values V_τ and W_τ to those values obtained from the fit to the total density of reactive states, and we determined values of $N_{\tau n}$ using linear least squares. Since $N_{\tau n}$ is the contribution from a given asymptotic channel to the total reactive flux, when we sum all the values of $N_{\tau n}$ for a particular threshold τ, we obtain the value of N_τ reported in the fit to the total reactive density.

Several representative fits to the state-selected reactive densities are shown in Fig. 2. In almost all of the fits, the first significant peak in the quantal densities is fit quite well, while the success of the fits in reproducing subsequent features, especially less prominent ones, is uneven. The latter may result because the mix of channels contributing the flux through a particular transition state may vary at energies above the threshold to which it corresponds.

The fits do not account for the strong minima at energies near the $[10^0]$ feature and just below the $[20^0]$ feature since there are no other thresholds at these energies. The minima just below the $[20^0]$ feature cause the fit to yield unphysical negative $N_{\tau n}$ values for the $[06^0]$ threshold. One possible explanation for these minima, mentioned earlier, is that they are due to trapped states. Isolated narrow resonances can lead to both dips and peaks in state-to-state transition probabilities, depending on the background scattering matrix.[16] Since state-selected densities are sums of energy-derivatives of state-to-state transition probabilities, it is possible that the effect of a trapped state upon a state-selected density could be manifested as a minimum.

In order to measure the contribution to the total reactive flux due to each initial channel quantitatively, we computed the ratio of $N_{\tau n}$ to N_τ for each initial channel n and each threshold τ. For each threshold, we determined all the channels which contribute at least 5% to the total reactive flux and then we arranged these channels in order of decreasing contributions. We then began summing these contributions, starting with the largest, until the sum first exceeded 75%. Those channels whose contribution are included in this subtotal are indicated in Fig. 5. The solid and dashed lines represent stretch adiabatic and non-adiabatic couplings of the initial channels with the thresholds. We clearly see that couplings which are adiabatic in the stretch mode ($v = v_1$) are strongly favoured. Stretch non-adiabaticity only begins to be significant for high v_1 within a given bend (v_2) manifold and for high v_2 within a given stretch (v_1) manifold.

These trends are made more quantitative in Table 2. The data compiled in this table include all channels which contribute at least 5% of the total reactive flux. M_{ad} and M_{nonad} are the number of initial channels which make stretch adiabatic and stretch non-adiabatic contributions, respectively, to the total reactive flux. The number of channels for which the ratio of $N_{\tau n}$ to N_τ is less than -0.05 is shown in parentheses; such contributions of course cannot be interpreted by transition-state theory. The values of M_{ad} and M_{nonad} confirm the conclusions we have given above from inspection of Fig. 5 regarding half-collision stretch adiabaticity, *i.e.* stretch non-adiabaticity is only significant for high-stretch and high-bend thresholds. It is interesting that the $[20^0]$ threshold exhibits an anomalously high degree of stretch non-adiabaticity; this may be due to trapped states.

Table 2 shows that there is a good correlation between j and v_2. The table shows the contributions to the total reactive flux through a given threshold with the contributions classified according to the value of $|j - v_2|$ for initial channels which make positive

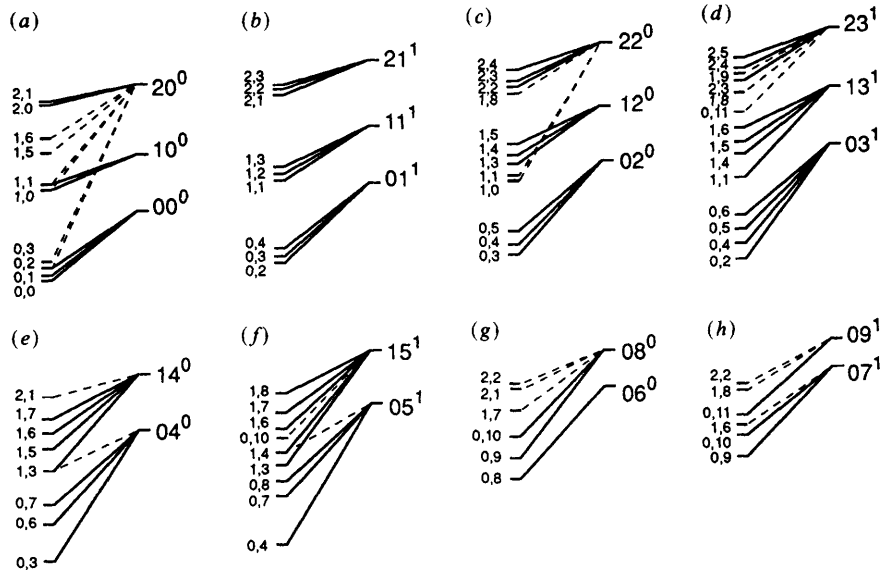

Fig. 5 Channels making significant contributions to the total reactive flux passing through each threshold for $J=0$ and $JP=1+$. Channels are labelled v, j and thresholds $v_1 v_2^K$. The quantum number l, which is equal to j for $J=0$ and $JP=1+$, is suppressed. The solid and dashed lines represent, respectively, stretch adiabatic and non-adiabatic contributions in half collisions. (*a*) $J=0$: $v_1=0,1,2$; $v_2=0$. (*b*) $JP=1+$: $v_1=0,1,2$; $v_2=1$. (*c*) $J=0$: $v_1=0,1,2$; $v_2=2$. (*d*) $JP=1+$: $v_1=0,1,2$; $v_2=3$. (*e*) $J=0$: $v_1=0,1$; $v_2=4$. (*f*) $JP=1+$: $v_1=0,1$; $v_2=5$. (*g*) $J=0$: $v_1=0$; $v_2=6,8$. (*h*) $JP=1+$: $v_1=0$; $v_2=7,9$

stretch adiabatic contributions larger than 5% in half collisions. When several channels with the same $|j-v_2|$ contribute, we indicate the number of channels in brackets and tabulate the sum of their percentage contributions. First, we observe that values of $|j-v_2|\leq 3$ are strongly preferred for all of the thresholds. In general, channels for which $|j-v_2|=1$ or 2 make dominant contributions. This is clearly demonstrated in Table 3 by the value of the average coupling strength, which is the average percentage contribution for a given $|j-v_2|$ to the ten thresholds for $JP=0+$ or $1+$, and the value of the significant coupling probability, which is the number of channels contributing more than +5% for a given $|j-v_2|$ divided by the total number of energetically accessible channels in the relevant vibrational manifold. In Table 2 we see that smaller values of $|j-v_2|$ are favoured by ground bend thresholds and larger values of $|j-v_2|$ become more important as v_2 increases. We did not find a significant correlation between j and v_2 for stretch non-adiabatic contributions to the reactive flux in half collisions; values of $|j-v_2|$ are more widely scattered.

$J=1$

Plots of N_{12}^1 and ρ_{12}^1 are given as the solid lines in Fig. 3(*a*) and (*b*), and individual-parity contributions to the density are shown in Fig. 3(*c*) and (*d*). The identification of all of the quantized transition states is more difficult for $J>0$ than for $J=0$ because the density of states is higher. Odd bend quantum numbers v_2 become allowed for non-zero values of total angular momentum. (Recall that $K\leq J$ and $K=v_2, v_2-2, v_2-4, \ldots 0$ or 1.) Eqn. (5) and the spectroscopic constants presented in the previous section show that the $[1v_2^K]$ thresholds lie very close in energy to the $[0(v_2+3)^{|K-1|}]$ thresholds.

Asymptotic channels are found in one or the other parity block based on the value $P=(-1)^{j+l}$. For transition states, the parity depends on J and K. The total parity is

Table 2 State-selected contributions to the total reactive flux passing through thresholds

					$\lvert j-v_2\rvert$ for $v=v_1$					
J	P	threshold	M_{ad} [a]	M_{nonad} [a]	0	1	2	3	4	>4
0	+	[00^0]	4	0	22[b]	41	27	9	0	0
		[02^0]	5	0	0	21	42 [2][c]	23	6	0
		[04^0]	5	2	0	19 [2]	29	26	7	0
		[06^0]	7 (4)	2 (5)	9	30 [2]	81	6	7	6
		[08^0]	2	8 (1)	0	11	28	0	0	0
		[10^0]	3	0	33	51	20	0	0	0
		[12^0]	5	1	7	34	37 [2]	10	0	0
		[14^0]	5 (1)	5 (2)	0	28 [2]	36 [2]	12	0	0
		[20^0]	2	6	13	17	0	0	0	0
		[22^0]	4	3	9	31	24 [2]	0	0	0
1	+	[01^1]	4	0	15	35	32	15	0	0
		[03^1]	6	0	0	23 [2]	41 [2]	25	8	0
		[05^1]	6	1 (1)	0	17 [2]	31	28	12 [2]	0
		[07^1]	6 (1)	4 (3)	8	20 [2]	42	19	0	7
		[09^1]	4 (3)	6 (5)	13	26	28	0	0	9
		[11^1]	3	0	24	45	26	0	0	0
		[13^1]	6	1	5	35 [2]	43 [2]	12	0	0
		[15^1]	5	2 (2)	0	22 [2]	37 [2]	9	0	0
		[21^1]	3	2 (2)	28	41	13	0	0	0
		[23^1]	3	3	7	22	16	0	0	0
1	−	[00^0]	6	0	21	41 [2]	27 [2]	6	0	0
		[01^1]	7	0	14 [2]	36 [2]	35 [2]	10	0	0
		[02^0]	7	0	0	20 [2]	43 [3]	24 [2]	0	0
		[03^1]	9	0	0	17 [2]	53 [4]	33 [2]	5	0
		[04^0]	7	0	0	15 [2]	35 [2]	40 [2]	8	0
		[05^1]	7	2 (3)	0	0	20 [2]	37 [2]	13 [2]	10
		[10^0]	5	0	36	52 [2]	19 [2]	0	0	0
		[11^1]	6	0 (4)	43 [2]	65 [2]	29 [2]	0	0	0
		[12^0]	6	1 (1)	8	51 [2]	46 [3]	0	0	0
		[20^0]	3	5	8	13 [2]	0	0	0	0
		[21^1]	5	2	26 [2]	41 [2]	9	0	0	0
		[22^0]	8	1	18 [2]	41 [4]	20 [2]	0	0	0

[a] M_{ad} and M_{nonad} are the number of initial channels with $v=v_1$ and $v\neq v_1$, respectively, that have $N_{\tau n}>0.05\ N_\tau$. The number in parentheses is the number of initial channels making negative contributions with $|N_{\tau n}|>0.05\ N_\tau$. [b] For example, 22 refers to the percentage of the total reactive flux passing through [00^0] at its threshold which originates from channels with $|j-v_2|=0$ and $v=v_1=0$. Only percentages ≥5% are included. [c] When several initial channels with the same value of $|j-v_2|$ make positive contributions ≥5%, the number of such channels is indicated in brackets and the sum of their percentage contributions is tabulated.

the product of the parities of the rotational and vibrational wavefunctions. The total parity of the rotational wave function is $(-1)^J=-1$. When $K=0$, the vibrational wave-function has even parity. When $K>0$, the bending mode v_2 is doubly degenerate with one even-parity and one odd-parity component.[17] As a result, for $J=1$, transition states having $K=0$ will appear only in the odd-parity density curve ρ_{12}^{1-}, while transition states having $K=1$ will appear in both the even-parity and the odd-parity curves.

Quantum numbers for the transition states associated with the features in ρ_{12}^{1+} and ρ_{12}^{1-} were assigned using the same techniques as for $J=0$, as discussed below. The $JP=1+$ and $J=0$ spectra are strikingly similar. This is because only transition states

Table 3 State-selected contributions to total reactive flux averaged over thresholds

			$\lvert j - v_2 \rvert$ for $v = v_1$					
	J	P	0	1	2	3	4	>4
average coupling strength	0	+	9	28	32	9	2	1
	1	+	10	29	31	11	2	2
significant coupling probability	0	+	0.60	0.76	0.76	0.43	0.25	0.06
	1	+	0.70	0.75	0.76	0.35	0.23	0.10

with even v_2 are allowed for $J = 0$ and only those with odd v_2 for $JP = 1+$, so that the density of states is the same in both cases and features are shifted by one quantum in v_2. The $J = 1$ thresholds are also slightly shifted up in energy from the $J = 0$ thresholds by a rotational energy of 2.6 meV, calculated from the value of $B = 10.6\ \text{cm}^{-1}$.

Parity-specific state-selected spectra are shown for the first five channels for both parities in Fig. 4(*a*) and (*b*). The $JP = 1+$ spectra are very similar to the state-selected density curves for $J = 0$ shown in Fig. 1; in fact, the $J = 0$ and $JP = 1+$ spectra are almost interchangeable if the $[v_1 v_2^0]$ thresholds and (v, j, l) channels for $J = 0$ are identified with the $[v_1(v_2+1)^1]$ thresholds and $(v, j+1, l+1)$ channels for $JP = 1+$. This striking similarity is observed not only for the spectra shown in Fig. 1 and 4(*a*) but also for state-selected spectra for every open channel up to 1.6 eV.

For $JP = 1-$ there are nearly twice as many channels as for $JP = 1+$ because for every non-zero value of j there are two channels: $(v, j, l = j+1)$ and $(v, j, l = j-1)$. Fig. 4(*b*) shows that channels (0, 0, 1), (0, 1, 0) and (0, 1, 2) couple primarily to the $[00^0]$ threshold, and that channels (0, 2, 1) and (0, 2, 3) couple to both the $[00^0]$ and the $[01^1]$ thresholds.

In Fig. 4(*c*), the double peak in the (1, 7, 7) spectrum shows that this channel couples to the $[21^1]$ and the $[15^1]$ thresholds. This structure most definitively locates the $[15^1]$ threshold. In Fig. 4(*d*), the state-selected spectrum for the (1, 8, 9) channel exhibits a maximum at 1.596 eV, as indicated by the unlabelled arrow between the $[22^0]$ and $[23^1]$ thresholds. This maximum is due to the $[16^0]$ threshold, whose spectroscopically predicted energy is 1.602 eV. The fit to ρ_{12}^{1-} does not find this threshold, presumably because its contribution is too highly overlapped with the final peak to be resolved.

The reactivity spectrum for each parity was fit by a sum of lineshapes appropriate for tunnelling through parabolic potential energy barriers as in eqn. (4). Because the $JP = 1+$ fit is relatively insensitive to the precise location of the $[15^1]$ and $[09^1]$ threshold energies, it was fitted constraining the V_τ values of the $[15^1]$ and $[09^1]$ thresholds to the energies of the maxima in the state-selected spectra for channels (1, 7, 7) and (0, 10, 10), respectively. In an initial fit where all of the W_τ, N_τ and V_τ values (except V_τ for $[15^1]$ and $[09^1]$) were allowed to vary, five N_τ values, including the last feature, were larger than 1.0. The first four of these N_τ values were then constrained to 1.0, and the fit was repeated. The threshold parameters V_τ and W_τ obtained in this second fit were then held fixed, and all N_τ values were determined by linear least squares.

The $JP = 1-$ reactivity spectrum was more difficult to fit because the density of states is twice as large as for $JP = 1+$. As for $J = 0$ and $JP = 1+$, the fitting procedure involved several steps. In the $JP = 1-$ fits, all of the V_τ and W_τ parameters for the odd v_2 thresholds were fixed to the values obtained in the final fit for $JP = 1+$. We assumed that the two thresholds with the same v_1, v_2, and K but different parity have the same effective potential-energy barrier height and width. The parameters of the last feature at 1.64 eV were not constrained. In the first step we carried out a fit with unconstrained N_τ values. Then all N_τ values except that for the highest-energy feature were constrained

to be no greater than one. Finally, *all* 20 pairs of threshold parameters V_τ and W_τ were constrained to the values obtained in step two, and all N_τ values were obtained by linear least squares. The synthetic density plots from the final fits for both parities are shown as the dashed lines in Fig. 3(*c*) and (*d*). Summing the synthetic densities for both parities yields the dashed curve in Fig. 3(*b*) for $J=1$, which upon integration results in the $J=1$ synthetic CRP curve shown as the dashed line in Fig. 3(*a*). The synthetic fits reproduce the quantal spectra exactly to within plotting accuracy. The agreement is particularly remarkable for $JP=1-$ since there are 20 thresholds to fit. This demonstrates that even when the density of states is high, the quantum-mechanical reactive flux from reactants to products is channelled through discrete transition states with assignable quantum numbers. The values of V_τ, N_τ and W_τ obtained from the fits to ρ_{12}^{1+} and ρ_{12}^{1-} are shown in Table 1. The strong correlation between the W_τ values of $J=0$ and $JP=1-$ $[v_1 v_2^K]$ thresholds validates the assumptions we have made in the fit to the $JP=1-$ reactive density.

After fitting the density of reactive states spectra for $JP=1+$ and $1-$, we fit the state-selected densities for both parities in a manner analogous to $J=0$. The coupling diagram for $JP=1+$, using the 75% criterion detailed above, is displayed in Fig. 5. The same trends are evident for $JP=1+$ as for $J=0$, namely that stretch adiabatic contributions are dominant in half collisions, especially for thresholds with low values of v_1 and v_2. For thresholds with higher values of v_1 and v_2, stretch non-adiabaticity becomes more significant, as was the case for $J=0$. For $JP=1-$, we find that half collisions between initial channels and transition states whose threshold energies are less than 1.25 eV are predominantly stretch adiabatic at the threshold energies. The $N_{\tau n}$ values for energetically higher-lying thresholds cannot be interpreted with as much confidence because the high density of states in this region makes it difficult to accurately fit the state-selected spectra. This is particularly true for the high-lying $v_1=0$ and 1 thresholds because they are highly excited in v_2 and they give rise to wide, overlapping features. We have more confidence, however, in the values of $N_{\tau n}$ for the $v_1=2$ thresholds, for which ratios of $N_{\tau n}$ to N_τ less than -0.05 were not observed. Since the trends for the lower-energy $JP=1-$ thresholds agree with those for $J=0$ and $JP=1+$, and the results for higher-energy thresholds must be treated with caution, the $JP=1-$ couplings are not included in Fig. 5.

The numbers of stretch adiabatic and non-adiabatic couplings in half-collisions for each transition state for $JP=1+$ and $1-$ are shown in Table 2. We also tabulate the percent contributions for a given $|j-v_2|$ with $v=v_1$. The results presented for $JP=1-$ are limited to transition states $[v_1=0\ v_2\leqslant 5]$, $[v_1=1\ v_2\leqslant 2]$ and $[v_1=2\ v_2\leqslant 2]$ for the reasons listed above. The similarities among the findings for $JP=0+$, $1+$ and $1-$ are striking. Stretch adiabatic couplings in half collisions are strongly preferred for all thresholds lying lower in energy than the $[06^0]$ threshold. When $JP=1+$ transition states $[v_1 v_2^1]$ are compared with $[v_1(v_2-1)^0]$ states for $J=0$, it is seen that the numbers of stretch adiabatic couplings M_{ad} are in nearly quantitative agreement, differing by one or less in every case but one. A greater number of such couplings is found for $JP=1-$ because there are twice as many channels. Trends in the contributions as functions of $|j-v_2|$ also show qualitative and in many cases quantitative agreement among the $JP=0+$, $1+$, and $1-$ thresholds. For example, when the percentage of reactive flux corresponding to various $|j-v_2|$ values for the $[00^0]$ threshold for $J=0$ is compared with that for $JP=1-$, we observe that the values for $|j-v_2|=1$ or 2 agree exactly, those for $|j-v_2|=0$ differ by only 1%, and those for $|j-v_2|=3$ differ by 3%. The high degree of quantitative agreement is particularly apparent for low bend states.

As noted earlier for $J=0$ thresholds, contributions to the total reactive flux from channels with larger $|j-v_2|$ values increase as v_2 increases for $JP=1+$ and $JP=1-$ thresholds. This trend is strikingly evident in the ground stretch manifold for $JP=1-$. Furthermore, the values of the average coupling strength and the significant coupling

probability in Table 3 for $J = 0$ and $JP = 1+$ are in nearly quantitative agreement. These quantities were not calculated for $JP = 1-$ because higher bend transition states were not included in Table 2 and this would skew the results.

In Table 1 are presented the V_τ values and the energies $E^{(1)}(v_1, v_2)$ calculated using eqn. (5) and the spectroscopic constants reported in the previous section. The calculated energies $E^{(1)}(v_1, v_2)$ are in good agreement with the fitted threshold energies V_τ, demonstrating the accuracy of the spectroscopic constants. The agreement is excellent for all the $[1\ v_2^K]$ thresholds and for the $[0\ v_2^K]$ and $[2\ v_2^K]$ thresholds with low v_2. Anharmonicity in the bending frequency increases as v_2 increases, and so the predicted spectroscopic energies, which include anharmonicity only to first order, tend to become less accurate for higher bend transition states.

The parameter W_τ is directly related to the force constant of the parabolic barrier associated with threshold τ and therefore is inversely related to the width of the potential barrier. In general, the value of W_τ increases with v_2 for transition states within a given v_1 manifold. This is consistent with the observation that the vibrationally adiabatic potential curve becomes narrower as v_2 increases (see paper I). This trend is most evident for the lowest four v_2 levels of the $v_1 = 0$ manifold and for the $v_1 = 1$ and 2 manifolds, where among 14 transition states the parameter W_τ fails to increase between successive v_2 levels only once. Furthermore, for the $K = 0$ transition states, which are common to both $J = 0$ and $JP = 1-$, there is a strong correlation between the W_τ values determined in the fits to the density of states. This gives us confidence in the assumption we made in the $JP = 1-$ density fit, namely that W_τ values for the $K = 1$ thresholds common to both $JP = 1+$ and $JP = 1-$ are the same. It is only for the $[04^0]$ and $[06^0]$ thresholds that the W_τ values from the $J = 0$ and $JP = 1-$ fits are not in good agreement; it is also among these bend levels that W_τ does not show a consistent tendency to increase with v_2. The reason for this lies in the difficulty in accurately fitting the features due to these two thresholds, which appear as broad shoulders in the $J = 0$ spectra and are strongly overlapped in the $JP = 1-$ spectra.

The fitting parameter N_τ would have a value of 1 in every case if each threshold were an ideal quantized transition state.[1,4-6] Most of the values of N_τ given in Table 1 are 1 or very nearly 1. The two values of 1.21 probably result from the difficulty in fitting overlapping features and the assumption of parabolic potential-energy barriers. By considering the two parity-specific portions of the $J = 1$ density of states, we separately see the contributions from the two degenerate odd-v_2 transition states. There is generally good agreement between the N_τ values of the two degenerate thresholds and in many cases N_τ is *ca.* 1; *i.e.* the transition states gate the reactive flux with unit efficiency. The N_τ value for the $J = 0$ or $JP = 1+$ threshold differs by more than 0.25 from the value for the corresponding $JP = 1-$ threshold in only four cases, namely $[06^0]$, $[07^1]$, $[13^1]$ and $[14^0]$. These are also the thresholds for which the trends discussed earlier for the state-selected $N_{\tau n}$ values and for the W_τ values are not clear. Features in the density spectra from these thresholds are more difficult to reproduce accurately owing to their broadness and to the large number of overlapping structures.

In general, the consistent trends among the N_τ and W_τ parameters for the $J = 0$, $JP = 1+$ and $JP = 1-$ thresholds indicate that the quality of the fit is very good. It is clear that for both $J = 0$ and $J = 1$, $H + H_2$ reactivity is globally controlled by quantized transition states.

4. Summary and Concluding Remarks

In an earlier paper,[1] we showed that the chemical reactivity of $H + H_2$ is globally controlled by a series of 10 thresholds for $J = 0$ at energies up to 1.6 eV. These thresholds are quantized dynamical bottlenecks, or transition states, that gate the flow of reactive flux from reactants to products. The transition states were identified and their quantum

numbers assigned by studying the energy dependence of the cumulative reaction probability and its derivative with respect to energy. In this paper we provided a similar analysis for the higher-density-of-states $J = 1$ case. In addition, for both $J = 0$ and 1, we identified the channels from which the reactive flux passing through the transition states at their thresholds originates. This was accomplished by fitting state-selected densities of reactive states using the transition-state parameters determined from the total cumulative reaction probability. We showed quantitatively that most initial channels proceed to the transition states adiabatically in the stretch vibrational quantum number. The tendency for stretch non-adiabatic coupling in half collisions increases with energy, particularly at energies above 1.2 eV. We also correlate rotational angular momentum quantum numbers j of the initial channels with the bend-vibrational quantum number v_2 of the transition state. We find that values of $|j - v_2| \leqslant 3$ are strongly preferred for stretch adiabatic couplings, and that the larger values of $|j - v_2|$ become more important for higher v_2. Threshold energies, parameters for the fitted effective potential-energy barriers, and trends in the state-selected coupling to transition states are highly consistent among the $J = 0$ case and the even- and odd-parity $J = 1$ cases.

The authors are grateful to Gillian C. Lynch for assistance with the calculations. This work was supported in part by the National Science Foundation, Minnesota Supercomputer Institute, and the Army High Performance Computing Research Center.

References

1 D. C. Chatfield, R. S. Friedman, D. G. Truhlar, B. C. Garrett and D. W. Schwenke, *J. Am. Chem. Soc.*, 1991, **113**, 486.
2 D. G. Truhlar and B. C. Garrett, *Annu. Rev. Phys. Chem.*, 1984, **35**, 159.
3 See also the step-like structures in the cumulative reaction probabilities of K. Haug, D. W. Schwenke, D. G. Truhlar, Y. Zhang, J. Z. H. Zhang and D. J. Kouni, *J. Chem. Phys.*, 1987, **87**, 1892 and unpublished, for the reaction of O with H_2, as discussed in: J. M. Bowman, *Chem. Phys. Lett.*, 1987, **141**, 545.
4 R. A. Marcus, *J. Chem. Phys.*, 1967, **46**, 959.
5 D. G. Truhlar, *J. Chem. Phys.*, 1970, **53**, 2041.
6 B. C. Garrett and D. G. Truhlar, *J. Phys. Chem.*, 1979, **83**, 1052; 1079; D. G. Truhlar, A. Isaacson and B. C. Garrett, in *Theory of Chemical Reaction Dynamics*, ed. M. Baer, CRC Press, Boca Raton, 1985, p. 65.
7 S. A. Cuccaro, P. G. Hipes and A. Kuppermann, *Chem. Phys. Lett.*, 1989, **157**, 440.
8 S. Califano, *Vibrational States*, John Wiley, London, 1976, p. 271.
9 A. J. C. Varandas, F. B. Brown, C. A. Mead, D. G. Truhlar and N. C. Blais, *J. Chem. Phys.*, 1987, **86**, 6258.
10 D. W. Schwenke, K. Haug, D. G. Truhlar, Y. Sun, J. Z. H. Zhang and D. J. Kouri, *J. Phys. Chem.*, 1987, **91**, 6080; D. W. Schwenke, K. Haug, M. Zhao, D. G. Truhlar, Y. Sun, J. Z. H. Zhang and D. J. Kouri, *J. Phys. Chem.*, 1988, **92**, 3202; D. W. Schwenke, M. Mladenovic, M. Zhao, D. G. Truhlar, Y. Sun and D. J. Kouri, in *Supercomputer Algorithms for Reactivity, Dynamics, and Kinetics of Small Molecules*, ed. A. Laganà, Kluwer, Dordrecht, 1989, p. 131.
11 M. Zhao, M. Mladenovic, D. G. Truhlar, D. W. Schwenke, O. Sharafeddin, Y. Sun and D. J. Kouri, *J. Chem. Phys.*, 1989, **91**, 5302; D. C. Chatfield, D. G. Truhlar and D. W. Schwenke, *J. Chem. Phys.*, in the press.
12 M. Zhao, M. Mladenovic, D. G. Truhlar, D. W. Schwenke, Y. Sun, D. J. Kouri and N. C. Blais, *J. Am. Chem. Soc.*, 1989, **111**, 852.
13 R. A. Marcus, *Discuss. Faraday Soc.*, 1967, **44**, 7.
14 See also: M. S. Child, *Discuss. Faraday Soc.*, 1967, **44**, 68 for a discussion of such correlations in coplanar collisions.
15 B. C. Garrett, D. W. Schwenke, R. T. Skodje, D. Thirumalai, T. C. Thompson and D. G. Truhlar, *ACS Symp. Ser.*, 1984, **263**, 375.
16 J. R. Taylor, *Scattering Theory*, Wiley, New York, 1972.
17 G. Herzberg, *Molecular Spectra and Molecular Structure. II. Infrared and Raman Spectra of Polyatomic Molecules*, D. van Nostrand, Princeton, 1945.

Paper 0/05693F; *Received* 18*th December*, 1990